

LETTER

A Compressive Regularization Imaging Algorithm for Millimeter-Wave SAIR

Yilong ZHANG^{†a)}, Nonmember, Yuehua LI^{†b)}, Member, Guanhua HE^{††}, and Sheng ZHANG^{††}, Nonmembers

SUMMARY Aperture synthesis technology represents an effective approach to millimeter-wave radiometers for high-resolution observations. However, the application of synthetic aperture imaging radiometer (SAIR) is limited by its large number of antennas, receivers and correlators, which may increase noise and cause the image distortion. To solve those problems, this letter proposes a compressive regularization imaging algorithm, called CRIA, to reconstruct images accurately via combining the sparsity and the energy functional of target space. With randomly selected visibility samples, CRIA employs l_1 norm to reconstruct the target brightness temperature and l_2 norm to estimate the energy functional of it simultaneously. Comparisons with other algorithms show that CRIA provides higher quality target brightness temperature images at a lower data level.

key words: millimeter wave, SAIR, compressive regularization, imaging algorithm

1. Introduction

Millimeter-wave imaging radiometer (MMIR) is a method of forming images through the passive detection of millimeter-wave radiation from a scene. It offers advantages over visible light and infrared imaging. Moreover, because of the significantly different brightness temperature between metal objects and the background, MMIR can be used to detect concealed metal objects in near-field. These benefits make MMIR an ideal imaging modality for remote sensing, safety check, and military applications [1].

However, current MMIR systems suffer from several limitations in terms of poor spatial resolution which is attained in size of antenna apertures. Aperture synthesis technology represents an effective approach to millimeter-wave radiometers for high-resolution observations with moderately sized antennas [2], [3].

SAIR measures the correlation between pairs of many nondirective antennas to achieve a larger aperture antenna, realizing high-resolution. Obviously, this approach meets the problem of big data processing, which traditional FFT and method based on the G matrix of SAIR cannot reduce.

In terms of solving contradictions between achieving larger aperture antenna and reducing the amount of data

processing, Compressive sensing (CS) theory is applied to G matrix method of SAIR via the sparsity of target brightness temperature images based on l_1 norm [4], [5]. But as non-adaptive measurements of CS, priori information is ignored which can help correct target brightness temperature images.

In this letter, we propose a compressive regularization imaging algorithm, called CRIA, for millimeter-wave SAIR to reconstruct images accurately via combining the sparsity (l_1 norm) and priori information which is the energy functional (l_2 norm) of target space [6]. Firstly, we randomly select part of visibility samples as we set the observation matrix is an identity matrix which is incoherence with DCT matrix. Then, the random number will help establish the basis matrix of target brightness temperature images which is made up of the G matrix of SAIR and DCT matrix. Brightness temperature images can be reconstructed by minimizing l_1 norm and l_2 norm of images simultaneously at last.

2. Model of Millimeter-Wave SAIR

Millimeter-wave SAIR measures the correlation value, namely the visibility function, between pairs of spatially separated antennas. Binary interferometer is the basic unit of SAIR. The geometric relationship of interferometry is shown in Fig. 1.

Antenna array is located on the plane $z = 0$ while the radiation source S is on the plane $z = R$. Assuming that the radiation source S is dispersed into N small parts. The visibility function can be expressed as:

$$V_{c,l} = \sum_{n=1}^N T(x_n, y_n) F_c(x_n, y_n) F_l^*(x_n, y_n) e^{-jK(R_c^c - R_n^l)} \Delta S_n \quad (1)$$

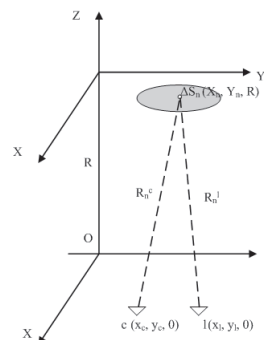


Fig. 1 Interference measurement schematic

Manuscript received December 27, 2014.

Manuscript revised March 19, 2015.

Manuscript publicized May 7, 2015.

[†]The authors are with School of Electronic and Optical Engineering, Nanjing University of Science and Technology, Nanjing, China.

^{††}The authors are with Huaihai Industrial Group Co., LTD., Shanxi, China.

a) E-mail: zhy1563@hotmail.com

b) E-mail: nlglyh2013@sina.cn (Corresponding author)

DOI: 10.1587/transinf.2014EDL8256

Where $T(x_n, y_n)$ is target brightness temperature images assuming that the interferometer is an ideal narrowband system, $F_c(x_n, y_n)$ and $F_l(x_n, y_n)$ are the normalized antenna pattern of antenna c and l. The distance R_n^c and R_n^l are processed approximately by Taylor expansion in far-field of SAIR, on which traditional FFT and G matrix method are established, so traditional FFT and G matrix method need phase compensation in near-field. Here, the distance R_n^c and R_n^l will be processed accurately to establish a new G matrix suitable for both far-field and near-field. Thus, Eq. (1) can be expressed as:

$$V_{c,l} = \sum_{n=1}^N T(n) F_c F_l^* e^{-jK\Delta R} \quad (2)$$

$$\Delta R = \sqrt{(x_n - X_c)^2 + (y_n - Y_c) + R^2} - \sqrt{(x_n - X_l)^2 + (y_n - Y_l) + R^2} \quad (3)$$

Hence rewrite Eq. (2) into the matrix form:

$$\mathbf{V}_{M \times 1} = \mathbf{G}_{M \times N} \mathbf{T}_{N \times 1} \quad (4)$$

$$G(m, n) = F_c(x_n, y_n) F_l^*(x_n, y_n) e^{j2\pi\Delta R_{mn}/\lambda} \quad (5)$$

$$\Delta R_{mn} = \sqrt{(x_n - X_{ml})^2 + (y_n - Y_{ml}) + R^2} - \sqrt{(x_n - X_{mc})^2 + (y_n - Y_{mc}) + R^2} \quad (6)$$

Based on Eq. (4), Eq. (5) and Eq. (6), CRIA will reconstruct target brightness temperature images accurately with part of visibility function.

3. Compressive Regularization Imaging Algorithm

Sparse representation has been a powerful approach to image restoration. The basic model of sparse representation in image denoising is expressed as:

$$\hat{\theta}_{ij} = \arg \min_{\theta_{ij}} \sum_{ij} \|\theta_{ij}\|_0 \text{ s.t. } D \cdot \theta = x \quad (7)$$

The image x can be approximated to a sparse linear combination of the columns with a basis matrix D. Thus we can recover a sparse approximation $\hat{\theta}$ for x by D. For target brightness temperature T of SAIR, Eq. (4) will be rewrote to:

$$\mathbf{V}_{M \times 1} = \mathbf{G}_{M \times N} \mathbf{D}_{N \times N}^T \mathbf{T}'_{N \times 1} \quad (8)$$

Where $D_{N \times N}$ is an orthonormal basis constructed by discrete cosine transform (DCT). In the actual measurement of SAIR, $\varepsilon^2(V : T)$ is the error functional and $E^2(T)$ is the energy functional, they are expressed as:

$$\varepsilon^2(V : T) = \|GT - V\|_F^2 \quad (9)$$

$$E^2(T) = \|T\|^2 \quad (10)$$

Based on the CS theory, the reconstruction method of SAIR can be expressed as:

$$\min \|T'\|_0 \text{ s.t. } \left\| \hat{\Phi} G D^T T' - \hat{V} \right\|_2 \leq \varepsilon \quad (11)$$

Where $\hat{\Phi}$ is constructed by m measurements vectors uniformly randomly selected from sensing matrix Φ which is the identity matrix. \hat{V} is the result of m measurements. Based on regularization with error functional and energy functional, reconstruction method of SAIR can be expressed as:

$$\min \|GT - V\|_2 \text{ s.t. } \|T\|_2 \leq E \quad (12)$$

CRIA employs l_1 norm to reconstruct the target brightness temperature and l_2 norm to estimate the energy functional of it simultaneously. Mathematically, the new functional of CRIA is expressed as:

$$L_{\lambda_1, \lambda_2}(V : T) = \left\| \hat{\Phi} G D^T T' - \hat{V} \right\|_2 + \lambda_1 \|T'\|_1 + \lambda_2 \|T'\|_2 \quad (13)$$

We explain each term of the new functional in detail as follows: The first and second terms are the reconstruction constraint. The reconstructed image should be consistent with the observation with respect to the imaging model and reconstructed by sparsest solution to reduce data calculation and denoising. The third term enforces the l_2 norm constraint as priori information and energy functional is considered, for T represents the intensity of radiation sources at millimeter-wave waveband, which can be estimated priori. Thus CRIA aims to solve:

$$\min L_{\lambda_1, \lambda_2}(V : T) \quad (14)$$

The proposed functional of CRIA involves nonsmooth and nonseparable l_1 norm terms which is hard to be minimized directly. Thus, CRIA adopts k-th gradient iteration to solve the minimization problem in cooperation with l_2 norm [7]. The main idea is tantamount to convert the unconstrained minimization problem into several easy constrained convex problems. Set function as:

$$f(X) = \left\| \hat{\Phi} G D^T X - \hat{V} \right\|_2 \quad (15)$$

$f(X)$ is a smooth convex function and is continuously differentiable with Lipschitz gradient. So,

$$X_k = \arg \min_X \{f(X_{k-1}) + \langle X - X_{k-1}, \nabla f(X_{k-1}) \rangle + \frac{1}{2t_k} \|X - X_{k-1}\|_2\} \quad (16)$$

where t_k equals to reciprocal of Lipschitz constant of function $f(X)$. Thus Eq. (14) becomes:

$$T'_k = \arg \min_{T'} \{f(T'_{k-1}) + \langle T' - T'_{k-1}, \nabla f(T'_{k-1}) \rangle + \frac{1}{2t_k} \|T' - T'_{k-1}\|_2 + \lambda_1 \|T'\|_1 + \lambda_2 \|T'\|_2\} \quad (17)$$

Or equivalently:

$$T'_k = \arg \min_{T'} \left\{ \frac{1 + 2\lambda_2 t_k}{2t_k} \|T' - C_k\|_2 + \lambda_1 \|T'\|_1 \right\} \quad (18)$$

Where

Table 1 CRIA algorithm.

Input: $\hat{\Phi}, \hat{V}, K, \lambda_1, \lambda_2, D, N$.
Output: target brightness temperature T .
Algorithm:
Step 1: calculate $\hat{\Phi} \cdot G \cdot D^T$ according to Eq. (4);
Step 2: set $k = 1, T'_{k-1} = \text{zero}(N)$;
Step 3: update by using Eqs. (15), (20);
Step 4: $k + 1$, if $k < K$, repeat from step 3, otherwise go to step 5;
Step 5: calculate T by using $T = D^T \cdot T'$

$$C_k = \frac{T'_{k-1} - t_k \nabla f(T'_{k-1})}{1 + 2\lambda_2 t_k} \quad (19)$$

Equation (18) can be divided into N constrained convex problems which can be solved respectively. Thus original nonsmooth and nonseparable l_1 norm terms could be solved easily. The solution of Eq. (18) is:

$$T'_k = \max\{|C_k| - \frac{\lambda_1 t_k}{1 + 2\lambda_2 t_k}, 0\} \times \text{sign}(C_k) \quad (20)$$

Then unconstrained minimization problem of CRIA can be easily solved by Eq. (15) and Eq. (20). CRIA is summarized in Table 1.

4. Experimental Results

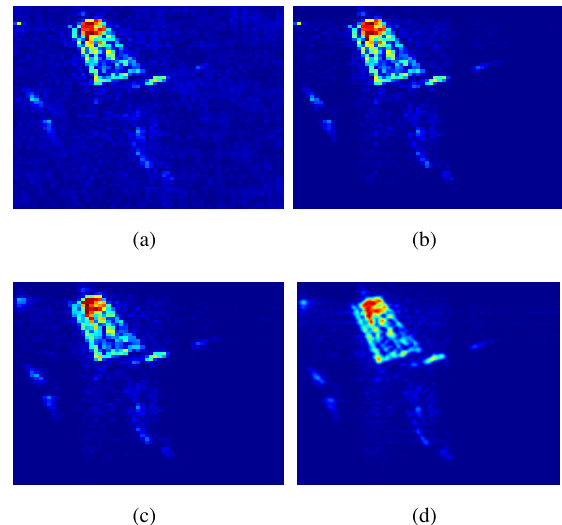
In this section, we demonstrate the performance of the CRIA and give the image and numerical comparison with the similar algorithm: MFFT, method based on G matrix and CS method with the same parameters of SAIR with different noise levels. Among the compared algorithms, only the CS method supports images reconstruction with part of visibility samples while MFFT, method based on the G matrix need entire visibility samples. In order to be able to include MFFT and method based on the G matrix in the comparisons, we perform two simulation experiments.

The performance of all methods is evaluated by using a 64×64 square image of ideal target brightness temperature distribution of plane shown in Fig. 2 which will be formulated as a vector (4096×1) by all algorithms. The gray value of images represents the intensity of radiation sources at frequency of 34GHz with an ideal bandwidth of 200MHz, where the metal plane has a minimum brightness temperature compared with the background. CRIA will reconstruct brightness temperature of the whole scene more accurately with this priori information. Parameters of SAIR are established in Table 2. Based on Eq. (4), the number of visibility samples ($M = 2500$) equals to the number of the row vector of G matrix, which also means CS method CRIA just need to calculate the corresponding row vector of G matrix based on Eq. (5) and Eq. (6) according to the selected part of visibility samples, that means a great reduction of the data processing. We use the peak signal-to-noise ratio (PSNR) as an objective measure of reconstruction quality and the zero-mean white Gaussian noise as received noise.

In first experiments, reconstruction images of Fig. 2 by MFFT and G matrix using entire visibility samples, CS

**Fig. 2** Ideal scene of target brightness temperature distribution of plane**Table 2** Simulation parameters of SAIR.

Simulation parameters	value
Center frequency	34GHz
scene size	1m \times 1m
image pixel size	64 \times 64
gray value of image	0~1
Imaging distance	10m
Antenna array	70 \times 70
minimum antenna spacing	24mm
Entire G size	2500 \times 4096
visibility samples	50 \times 50
variance of received noise	0~0.14

**Fig. 3** Reconstruction images of plane. (a), (b), (c), (d) are reconstructed by MFFT, G matrix, CS with 70% of visibility samples, CRIA with 70% of visibility samples, respectively.

method and CRIA using 70% of visibility samples without noise are shown in Fig. 3. CRIA produces a more visually pleasing result, compared with the results of other methods. The PSNR performance of all methods of reconstruction images of Fig. 2 with different variance Gaussian noise is shown in Fig. 4, while CRIA and CS still use 70% of visibility samples. We can see that the PSNR performance of CRIA is the best with any different variance Gaussian noise compared to the other three. And with the increase of Gaussian noise, PSNR performance of CRIA decreases much more slowly, which means CRIA has strong ability of denoising.

In second experiments, CS and CRIA are evaluated by

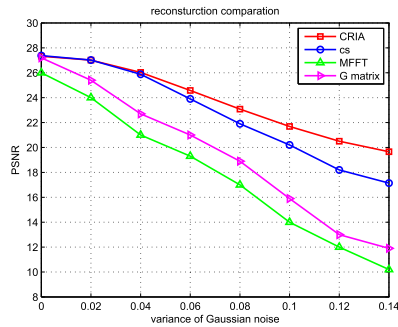


Fig. 4 Mean reconstruction PSNR comparison for all algorithms with different variance Gaussian noise

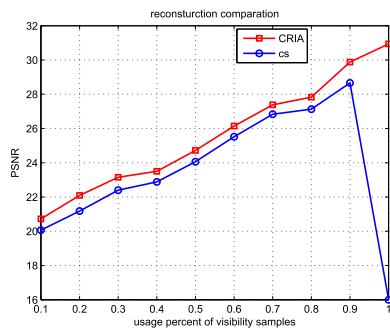


Fig. 5 Mean reconstruction PSNR comparison for CS and CRIA with different usage percent of visibility samples

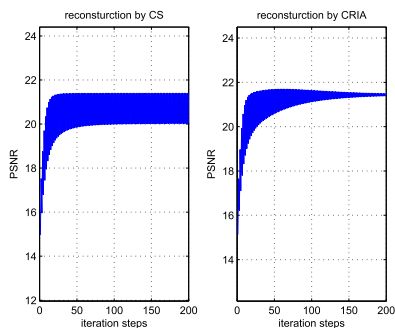


Fig. 6 Reconstruction PSNR comparison for CS and CRIA with 200 iteration steps

different usage percent of visibility samples ranging from 10% to 100%, the PSNR performance of them for the reconstruction images of Fig. 2 without noise is shown in Fig. 5. The PSNR performance of CRIA is better than CS without received noise of any usage percent of visibility samples and while using entire visibility samples, CS even cannot work.

With variance Gaussian noise is 0.1, we do comparisons of CS and CRIA in different number of iterations and the result is shown in Fig. 6. Result shows the PSNR performance of CS is unstable with interference by noise and CRIA is more robust.

5. Conclusion

In this letter, we have proposed a compressive regularization imaging algorithm, called CRIA, for millimeter-wave SAIR to reconstruct images via combining the sparsity and priori information. With randomly selected visibility samples, CRIA reconstruct images by minimizing l_1 norm and l_2 norm of target brightness temperature images simultaneously. Experimental results demonstrate that CRIA provides higher quality target brightness temperature images at a lower data level and performs very robustly with received noise. In the current model, CRIA formulates brightness temperature images as a vector which limits the image size and future work incorporating structured matrix completion to CRIA is being developed.

Acknowledgements

The authors would like to thank the anonymous reviewer and editors for their helpful comments and suggestions. This work is supported by National Natural Science Foundation of China under Grants 61371038, National Ministry Foundation of China under Grants 9140A05070910BQ02 and Postdoctoral Research Fund Plan of Jiangsu Province under Grants 1302027C.

References

- [1] N. Gopalsami, S. Bakhtiari, T.W. Elmer, and A.C. Raptis, "Application of Millimeter-Wave Radiometry for Remote Chemical Detection," *IEEE Trans. Microw. Theory Tech.*, vol.56, no.3, pp.700–709, 2008.
- [2] I. Ramos-Perez, G.F. Forte, A. Camps, X. Bosch-Lluis, E. Valencia, N. Rodriguez-Alvarez, H. Park, and M. Vall-llosera, "Calibration, Performance, and Imaging Tests of a Fully Digital Synthetic Aperture Interferometer Radiometer," *IEEE J. SEL. TOP APPL. EARTH. OBS.*, vol.5, no.3, pp.723–734, 2012.
- [3] I. Corbella, N. Duffo, M. Vall-llosera, A. Camps, and F. Torres, "The visibility function in interferometric aperture synthesis radiometry," *IEEE Trans. Geosci. Remote Sens.*, vol.42, no.8, pp.1677–1682, Aug. 2004.
- [4] S. Li, X. Zhou, B. Ren, H.-J. Sun, and X. Lv, "A compressive sensing approach for synthetic aperture imaging radiometer," *Progress In Electromagnetics Research*, vol.135, pp.583–599, 2013.
- [5] J. Chen and Y. Li, "The CS-Based imaging algorithm for near-Field synthetic aperture imaging radiometer," *IEICE Trans. Electron.*, vol.E97-C, no.9, pp.911–914, Sept. 2014.
- [6] M. Joshi and A. Jalobeanu, "MAP estimation for multiresolution fusion in remotely sensed images using an IGMRF prior model," *IEEE Trans. Geosci. Remote Sens.*, vol.48, no.3, pp.1245–1255, March 2010.
- [7] A. Beck, A. Ben-Tal, and L. Tetrushvili, "A sequential parametric convex approximation method with applications to nonconvex truss topology design problems," *Journal of Global Optimization*, vol.47, no.1, pp.29–51, 2010.